Corneal wave aberration from videokeratography: accuracy and limitations of the procedure

Antonio Guirao and Pablo Artal

Laboratorio de Optica, Departamento de Física, Universidad de Murcia, Campus de Espinardo (Edificio C), 30071 Murcia, Spain

Received August 30, 1999; revised manuscript received January 23, 2000; accepted February 1, 2000

A procedure to calculate the wave aberration of the human cornea from its surface shape measured by videokeratography is presented. The wave aberration was calculated as the difference in optical path between the marginal rays and the chief ray refracted at the surface, for both on- and off-axis objects. The corneal shape elevation map was obtained from videokeratography and fitted to a Zernike polynomial expansion through a Gram–Schmidt orthogonalization. The wave aberration was obtained also as a Zernike polynomial representation. The accuracy of the procedure was analyzed. For calibrated reference surface elevations, a root-mean-square error (RMSE) of 1 to 2 μm for an aperture 4–6 mm in diameter was obtained, and the RMSE associated with the experimental errors and with the fitting method was 0.2 μm. The procedure permits estimation of the corneal wave aberration from videokeratoscopic data with an accuracy of 0.05–0.2 μm for a pupil 4–6 mm in diameter, rendering the method adequate for many applications. © 2000 Optical Society of America [S0740-3232(00)01205-9]

OCIS codes: 330.4460, 330.5370, 330.7310, 080.1010.

1. INTRODUCTION

An accurate procedure to obtain the corneal aberrations from the corneal shape is required in different applications. In basic studies the corneal aberrations used in conjunction with those measured in the complete eye serve to estimate the relative sources of aberrations in the human eye[1] or can be incorporated into more elaborated schematic eye models.[2] In cases of relevant clinical interest, i.e., keratoconus[3,4] and corneal refractive surgery,[5,6] the corneal aberrations also provide important information.

The wave aberration of the cornea is modified by the internal ocular surfaces[1,7,8] to produce the final retinal image, and therefore measuring only the anterior corneal aberrations is not the most adequate procedure to evaluate the overall image quality in the eye. However, the cornea is the main refracting element and probably also a major contributor to the ocular aberrations.[9] Moreover, this will certainly be the case in abnormally aberrated corneas, such as those reported after refractive surgery.

The spherical aberration has been usually considered as the main aberration of the cornea,[9,10] in addition to the astigmatism, but since new corneal topography devices have permitted more detailed studies of the corneal surface, the importance of coma[11] and higher-order aberrations[12] has been revealed.

The first step in estimating the aberrations produced by the anterior surface of the cornea is to measure the cornea's shape accurately. In the early 1960's Jenkins already noted[10] the importance of having an instrument capable of measuring with precision the corneal curvature at each point. Various techniques have been proposed to measure the corneal topography: interferometry, ultrasonography, profile photography, and holography; but many of the devices in practical use today (e.g., videokeratoscopes) are based on the Placido disk principle. In this system, a series of concentric rings reflected on the cornea are imaged by a video camera and the corneal geometry is obtained in each meridian from the ring spacing. Several studies[13–15] that used calibrated surfaces showed that, owing to the approximations in the surface reconstruction computations, Placido-based devices do not accurately measure the corneal shape, in particular in the periphery and when the surface differs greatly from a sphere. In addition to the errors due to the reconstruction algorithms, other sources of inaccuracy arise from the measuring process, for instance, tilt between the optical axis of the cornea and the axis of the instrument, defocus in the ring image, and misalignments of the eye.

A second problem related to the determination of corneal aberrations is how to calculate them once the corneal surface is known. A direct approach is to obtain a remainder lens by subtracting the best conic surface fitted to the measured cornea and simply to calculate the aberrations by multiplying by the refractive-index difference.[16] However, this method neglects some aberration terms that can be important. Another alternative[11] uses an approximate (neglecting nonlinear terms) analytical expression that depends on the corneal surface.

We present here a further procedure to estimate the aberrations of the cornea from the corneal elevations measured with a videokeratoscope, and we analyze its accuracy in detail.

2. METHODS

A. Wave Aberration Associated with a Refracting Surface

This section presents a procedure to obtain the wave aberration associated with a given surface for point objects

located both on axis and off axis. Figure 1 shows a schematic representation of the image formation by a refracting surface separating two media of refractive indices n and n'. An object point at an arbitrary position $(x, y) = (p \sin\beta, p\cos\beta)$ on the plane XY has its image centered at the point $(x', y') = (-p' \sin\beta, -p' \cos\beta) = (x/m, y/m)$ of the paraxial plane $X'Y'$, where m is the magnification. A marginal ray intersects the system at some point (r, θ) of the exit pupil. Corresponding to this point, the surface has an elevation $z(r, \theta)$. The wave aberration (W) along a certain marginal ray is defined as the difference in optical path length between the ray under consideration, $\overline{d - d'}$, and the chief ray, $\overline{l - l'}$, passing through the center of the exit pupil[17]:

$$W = nd + n'd' - nl - n'l'. \tag{1}$$

These four distances may be written as

$$l = s(1 + Y^2)^{1/2}, \tag{2a}$$

$$l' = s'(1 + Y'^2)^{1/2}, \tag{2b}$$

$$d = s(1 + X^2 + Y^2 + Z^2 + 2Z - 2AXY)^{1/2}, \tag{3a}$$

$$d' = s'(1 + X'^2 + Y'^2 + Z'^2 - 2Z' + 2AX'Y')^{1/2}, \tag{3b}$$

with $X = r/s$ $(X' = r/s')$, $Y = p/s$ $(Y' = p'/s')$, $Z = z/s$ $(Z' = z/s')$, and $A = \sin(\theta + \beta)$.

An analytical expression for the wave aberration as a function of the surface elevation, up to the fourth order in pupil and object coordinates, is obtained from Eqs. (2a) and (2b), rewritten as $l \approx s[1 + (p^2/2s^2) - (p^4/8s^4)]$, when $p, r, z \ll s$, and from Eqs. (3a) and (3b) expressed as a Taylor expansion of three variables.[18] If we take the derivatives of the functions d and d' with respect to X, Y, and Z and rearrange terms, Eq. (1) for the wave aberration can be expressed as

$$\begin{aligned}
W(r, \theta; z) &= \left[\frac{n}{s} + \frac{n'}{s'} - n^2\left(\frac{1}{ns} + \frac{1}{n's'}\right)\sin^2\omega\right]\frac{r^2}{2} \\
&- \left(\frac{n}{s^3} + \frac{n'}{s'^3}\right)\frac{r^4}{8} + \frac{n(n'^2 - n^2)}{2n'^2} \\
&\times r(\cos\beta\sin\theta + \sin\beta\cos\theta)\sin^3\omega \\
&+ \frac{n^2}{4}\left(\frac{1}{n's'} + \frac{1}{ns}\right)r^2(\cos 2\beta\cos 2\theta \\
&- \sin 2\beta\sin 2\theta)\sin^2\omega + \frac{n}{2}\left(\frac{1}{s^2} - \frac{1}{s'^2}\right)r^3(\cos\beta\sin\theta \\
&+ \sin\beta\cos\theta)\sin\omega + (n - n')\left(1 + \frac{n}{2n'}\sin^2\omega\right)z \\
&+ n\left(\frac{1}{s} + \frac{1}{s'}\right)rz(\cos\beta\sin\theta + \sin\beta\cos\theta)\sin\omega \\
&+ \frac{n^2}{2}\left(\frac{1}{n's'} + \frac{1}{ns}\right)z^2\sin^2\omega + n\left(\frac{1}{s'^2} - \frac{1}{s^2}\right) \\
&\times rz^2(\cos\beta\sin\theta + \sin\beta\cos\theta)\sin\omega \\
&+ \left(\frac{n}{s^3} + \frac{n'}{s'^3}\right)\frac{r^2z^2}{2} + \left(\frac{n'}{s'^2} - \frac{n}{s^2}\right)\frac{r^2z}{2}.
\end{aligned} \tag{4}$$

Since we are interested in surfaces with a general ellipsoidal shape, similar to that of the cornea, we express the shape as a conic plus an asymmetric term:

$$z(r, \theta) = \frac{r^2}{2R} + \frac{r^4}{8R^3}K^2 + \frac{r^6}{16R^5}K^4 + \cdots + \Delta z(r, \theta), \tag{5}$$

where R is the base radius of curvature of the conic surface and K is a constant of asphericity, with $K > 0$ corresponding to an ellipsoid, $K < 0$ to a hyperboloid, $K = 0$ to a paraboloid, and $K = 1$ to a sphere. K is related with the eccentricity of the ellipsoid as $K^2 = 1 - e^2$. With expression (5), the wave aberration can be described as that of a conic surface plus asymmetric terms:

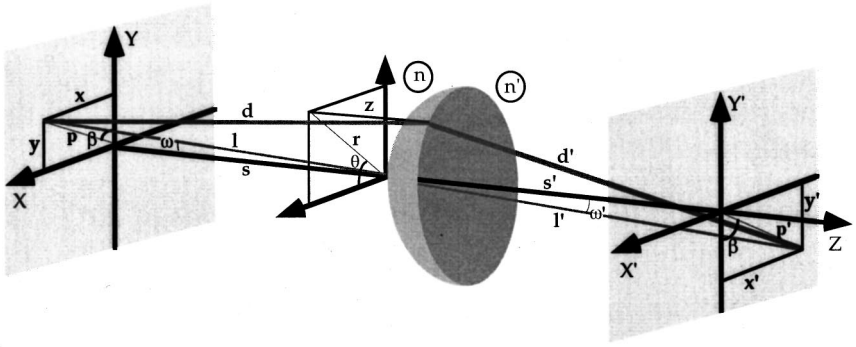

Fig. 1. Imaging of an off-axis point object by a refracting surface separating media of refractive indices n and n'. The exit pupil is located at the vertex of the surface.

$$W(r,\theta) = W_{\text{sphere}}(r,\theta) - \frac{e^2(n - n')}{8R^3} r^4 + [(n - n') + L \sin^2 \omega + Mr^2 + N(\cos\beta \sin\theta + \sin\beta \cos\theta) r \sin\omega]\Delta z + [T \sin^2 \omega + Ur^2 + V(\cos\beta \sin\theta + \sin\beta \cos\theta) r \sin\omega]\Delta z^2, \quad (6)$$

with

$$L = (n - n')\frac{n}{2n'}, \qquad M = \frac{1}{2}\left(\frac{n'}{s'^2} - \frac{n}{s^2}\right),$$

$$N = n\left(\frac{1}{s} + \frac{1}{s'}\right), \qquad T = \frac{n^2}{2}\left(\frac{1}{n's'} + \frac{1}{ns}\right),$$

$$U = \frac{1}{2}\left(\frac{n}{s^3} + \frac{n'}{s'^3}\right), \qquad V = n\left(\frac{1}{s'^2} - \frac{1}{s^2}\right).$$

The first term in expression (6) represents the wave aberration for a spherical refracting surface and can be expressed by

$$W_{\text{sphere}}(r,\theta) = a_d r^2 + a_s r^4 + a_t(\cos\beta\, r \sin\theta + \sin\beta\, r \cos\theta) + a_a(\cos 2\beta r^2 \cos 2\theta - \sin 2\beta r^2 \sin 2\theta) + a_c(\cos\beta r^3 \sin\theta + \sin\beta r^3 \cos\theta), \quad (7)$$

where

$$a_s = \frac{n - n'}{8R^3} + \frac{M}{2R} - \frac{U}{4},$$

$$a_d = \left(\frac{L}{2R} - T\right)\sin^2\omega - \frac{n'\Delta s'}{2s'^2},$$

$$a_t = \frac{n(n'^2 - n^2)}{2n'^2}\sin^3\omega,$$

$$a_c = \frac{1}{2}\left(\frac{N}{R} - V\right)\sin\omega, \qquad a_a = \frac{T}{2}\sin^2\omega$$

represent the coefficients of defocus, spherical aberration, distortion, astigmatism and coma, respectively. Defocus is introduced if the image is observed at a plane separated a distance $\Delta s'$ from the paraxial plane.

For objects on-axis ($\sin\omega = 0$), expression (6) is reduced to

$$W(r,\theta) = \frac{-n'\Delta s'}{2s'^2} r^2 + \left[a_{\text{sP}} + \frac{K^2(n - n')}{8R^3}\right] r^4 + (n - n')\Delta z + Mr^2\Delta z + U r^2 \Delta z^2, \quad (8)$$

$a_{\text{sP}} = (M/2R) - (U/4)$ being the spherical aberration for a paraboloid. Only a spherical aberration appears in this case for a refracting sphere.

B. Corneal Surface Shape As an Expansion of Zernike Polynomials

Most of the available videokeratoscopes measure the corneal curvature or the elevations or both at a sample of points along meridians having equal angular spacing. Although curvature maps are commonly used in clinical applications, elevation maps are more suitable in studies of the optical properties of the cornea.[19] Elevation maps represent the distance (z_i) from each point of the corneal surface to a reference plane tangential to the vertex of the cornea [Fig. 2(a)].

Elevation data may be expressed as a polynomial expansion. Zernike polynomials[20,21] are an orthogonal set providing a convenient mathematical representation for the corneal aberrations. The corneal surface expressed as a linear combination of L Zernike terms is[22]

$$z(\rho,\theta) = \sum_{j=1}^{L} a_j Z_j(\rho,\theta), \quad (9)$$

where $\rho = r/r_0$ is the normalized radial variable and θ is the angular variable over the pupil, Z_j is each Zernike polynomial, and a_j the coefficient. Table 1 lists the first 15 polynomials, corresponding to an expansion up to the fourth order, and its counterpart in a monomial representation.[23]

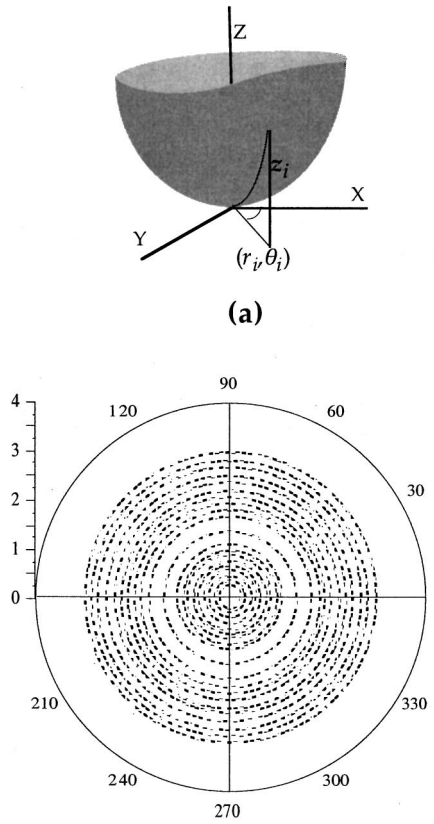

Fig. 2. (a) Elevation (z_i) of the corneal surface at the sampled point (r_i, θ_i) of the exit pupil. (b) Plane of reference and sample of points where the elevation is measured.

Table 1. First 15 Zernike Polynomials and Their Monomial Representation

Order	Zernike Polynomial	Monomial Representation
0	$Z_1 = 1$	1
First	$Z_2 = 2\rho\cos\theta$	x
	$Z_3 = 2\rho\sin\theta$	y
Second	$Z_4 = \sqrt{3}(2\rho^2 - 1)$	$-1 + 2(x^2 + y^2)$
	$Z_5 = \sqrt{6}\rho^2\cos 2\theta$	$x^2 - y^2$
	$Z_6 = \sqrt{6}\rho^2\sin 2\theta$	$2xy$
Third	$Z_7 = \sqrt{8}(3\rho^2 - 2)\rho\cos\theta$	$-2x + 3x(x^2 + y^2)$
	$Z_8 = \sqrt{8}(3\rho^2 - 2)\rho\sin\theta$	$-2y + 3y(x^2 + y^2)$
	$Z_{10} = \sqrt{8}\rho^3\cos 3\theta$	$x(x^2 - 3y^2)$
	$Z_{11} = \sqrt{8}\rho^3\sin 3\theta$	$y(3x^2 - y^2)$
Fourth	$Z_9 = \sqrt{5}(6\rho^4 - 6\rho^2 + 1)$	$1 + 6(x^4 + y^4 - x^2 - y^2 + 2x^2y^2)$
	$Z_{12} = \sqrt{10}(4\rho^2 - 3)\rho^2\cos 2\theta$	$-3(x^2 - y^2) + 4(x^4 - y^4)$
	$Z_{13} = \sqrt{10}(4\rho^2 - 3)\rho^2\sin 2\theta$	$2xy[-3 + 4(x^2 + y^2)]$
	$Z_{14} = \sqrt{10}\rho^4\cos 4\theta$	$x^4 - 6x^2y^2 + y^4$
	$Z_{15} = \sqrt{10}\rho^4\sin 4\theta$	$4xy(x^2 - y^2)$

Videokeratoscopy provides a finite number of values z_i for the corneal elevation [Fig. 2(b) shows an example], whereas Zernike polynomials are orthogonal only on the continuous unit circle domain, not over a discrete and finite sample of points (ρ_i, θ_i). Therefore it is not possible to calculate the expansion coefficients by using the advantages of orthogonality directly. There are several methods to deduce the coefficients when the function is sampled. The classical procedure has been the least-squares method, consisting in minimizing the expression $\Sigma_i[\Sigma_j a_j Z_j(\rho_i, \theta_i) - z_i]^2$ to obtain the coefficients a_j. Although, the least-squares method has been regarded as numerically unstable owing to matricial inversion process, it has been found stable with adequate sampling.[20] Another alternative that obtains each coefficient by straightforward numerical integration and by use of the orthogonal properties of the polynomials is not adequate because of the uniformly distributed sample and the excessive two-dimensional integration required.

A third procedure that generates a set of polynomials that are orthogonal on the finite and discrete sample allows us to keep the advantages of an orthogonal expansion.[20,22,24] This technique first requires the construction of the new set of polynomials, $V_j(\rho, \theta)$, from the Zernike ones. To find this intermediate set, we perform a Gram–Schmidt orthogonalization to generate the new polynomials through the iterative expression

$$V_j = Z_j + \sum_{s=1}^{j-1} D_{js} V_s, \tag{10}$$

with $D_{js} = -\Sigma_i Z_j V_s / \Sigma_i {V_s}^2$, $j = 2, 3, \ldots, L$, and $s = 1, 2, \ldots, j-1$. In a second step, corneal elevations are decomposed into a linear combination of the new polynomials:

$$z(\rho, \theta) = \sum_{j=1}^{L} b_j V_j(\rho, \theta). \tag{11}$$

The values of the coefficients b_j are computed simply as orthogonal projections: $b_j = \Sigma_i z_i V_j / \Sigma_i {V_j}^2$. Finally, by comparison with the Zernike expansion, the following relationship between coefficients b_j and Zernike coefficients (a_j) is obtained:

$$a_j = b_j + \sum_{k=j+1}^{L} a_k D_{kj}, \qquad a_L = b_L. \tag{12}$$

C. Zernike Representation of the Wave Aberration

From the elevation values $z(\rho_i, \theta_i)$, the exact wave aberration $W(\rho_i, \theta_i)$ is obtained at each point of the sampled surface by means of Eqs. (1)–(3). This set of values for the wave aberration may be fitted to Zernike polynomials by use of the same method as for fitting the corneal surface, producing the next expansion:

$$W(\rho, \theta) = \sum_{j=1}^{L} A_j Z_j(\rho, \theta). \tag{13}$$

When the refracting surface is expressed as a Zernike polynomial expansion, an alternative way to obtain the wave aberration in Zernike polynomials, which provides the functional dependencies, consists of introducing the right-hand side of Eq. (9) into Eq. (4). Coefficients for the aberrations are obtained as linear combinations of the Zernike coefficients for the surface when only the terms up to the fourth order are kept:

$$A_9 = (n - n')a_9 + \frac{{r_0}^4}{6\sqrt{5}} a_{\mathrm{sP}},$$

$$A_4 = \frac{6\sqrt{5}}{2\sqrt{3}} A_9 + \frac{1}{2\sqrt{3}} a_d {r_0}^2 + \frac{N r_0}{2\sqrt{3}}[(a_2 - \sqrt{8}a_7)\sin\beta + (a_3 - \sqrt{8}a_8)\cos\beta]\sin\omega,$$

$$A_{2(3)} = (n - n')a_{2(3)} + \left(\frac{a_t}{2} + \frac{a_c r_0^2}{3}\right) r_0 \underset{(\cos\beta)}{\sin\beta} + (n - n')\left(\frac{n}{2n'}\sin^2\omega + \frac{2}{3}\gamma\right)[a_{2(3)} - \sqrt{8}a_{7(8)}] + \frac{Nr_0}{\sqrt{6}}\left[-(a_5 - \sqrt{15}a_{12}) \underset{(\cos\beta)}{\sin\beta} + (a_6 - \sqrt{15}a_{13}) \underset{(\sin\beta)}{\cos\beta}\right]\sin\omega,$$

$$A_{5(6)} = (n - n')a_{5(6)} - \frac{a_a r_0^2}{\sqrt{6}} \underset{(\sin 2\beta)}{\cos 2\beta} + (n - n') \times \left(\frac{n}{2n'}\sin^2\omega + \frac{3}{4}\gamma\right)[a_{5(6)} - \sqrt{15}a_{12(13)}] + \frac{Nr_0}{2\sqrt{6}}\left[2(a_2 - \sqrt{8}a_7) \underset{(\cos\beta)}{\sin\beta} - 2(a_3 - \sqrt{15}a_8) \underset{(\sin\beta)}{\cos\beta}\right]\sin\omega,$$

$$A_{7(8)} = (n - n')a_{7(8)} + \frac{a_c r_0^3}{3\sqrt{8}} \underset{(\cos\beta)}{\sin\beta} + (n - n')\frac{2}{3\sqrt{8}}\gamma[a_{2(3)} - \sqrt{8}a_{7(8)}] + \frac{Nr_0}{\sqrt{48}}\left[(a_5 - \sqrt{15}a_{12}) \underset{(\cos\beta)}{\sin\beta} + (a_6 - \sqrt{15}a_{13}) \underset{(\sin\beta)}{\cos\beta}\right]\sin\omega,$$

$$A_{10(11)} = (n - n')a_{10(11)} + \frac{\sqrt{3}}{2\sqrt{4}}Nr_0\left[(a_5 - \sqrt{15}a_{12}) \underset{(\cos\beta)}{\sin\beta} - (a_6 - \sqrt{15}a_{13}) \underset{(\sin\beta)}{\cos\beta}\right]\sin\omega,$$

$$A_{12(13)} = (n - n')a_{12(13)} + (n - n') \times \frac{\sqrt{3}}{4\sqrt{5}}\gamma[a_{5(6)} - \sqrt{15}a_{12(13)}],$$

$$A_{14(15)} = (n - n')a_{14(15)}, \tag{14}$$

where $\gamma = (r_0^2 M)/(n - n')$ and r_0 is the radius of the pupil.

These expressions show how each coefficient expressing the surface affects the fourth-order aberration coefficients. Coefficient A_9 in Eq. (14) represents the spherical aberration and has two terms: The first appears if the surface is an ellipsoid, and the second corresponds to the spherical aberration of the paraboloid ($a_9 = 0$). The ideal conic surface for fourth-order aberrations ($A_9 = 0$) has an asphericity given by

$$K_0^2 = \frac{8R^3}{(n' - n)}a_{\mathrm{sP}}. \tag{15}$$

This value reduces to $K_0^2 = 1 - (n^2/n'^2)$ ($e_0 = n/n'$) when the object is at infinity. On the other hand, every term characterizing the surface passes directly to the aberration with the factor $(n - n')$. However, it is interesting to note the apparition of the off-axis and crossed terms. For instance, a tilted surface [$a_{2(3)} \neq 0$] generates coma [coefficients $A_{7(8)}$].

Coefficients A_j for the aberration depend on the parameter γ, i.e., of the distance s' to the image plane. Aberrations may be evaluated on a plane close to the paraxial one, in particular, on the plane of the best image that can be calculated by finding the value $\Delta s'$ that minimizes the Strehl ratio.[25] For not-very-large aberrations, the Strehl ratio is given approximately[17] by $\Pi_{j=2}^{L}\exp(-A_j^2)$. The best-image plane is determined by solving $\Sigma_{j=2}^{L}A_j(\mathrm{d}A_j/\mathrm{d}s') = 0$. Since the Zernike terms represent balanced aberrations, a valid approximation to this equation consists of calculating the value $\Delta s'$ that yields $A_4 = 0$ [defocus coefficient in Eq. (14)].

Often it is useful to refer to the primary or Seidel aberrations, represented as expansions of the first Zernike polynomials. Z_2 and Z_3 are tilt terms in the X and Y directions, respectively. The term Z_4 represents defocus. Z_5 and Z_6 contain defocus plus astigmatism along 0° and 45°. Z_7 and Z_8 represent coma and tilt, respectively. Z_9 represents spherical aberration plus defocus. Since in a general surface the coordinates of the aberrations may not be aligned in any specific direction with respect to the

Table 2. Aberration Seidel Coefficients in the Function of the Fourth-Order Zernike Coefficients

Name	Magnitude	Angle
Tilt	$A_t = 2[(A_2 - \sqrt{8}A_7)^2 + (A_3 - \sqrt{8}A_8)^2]^{1/2}$	$\theta_t = \arctan\dfrac{A_3 - \sqrt{8}A_8}{A_2 - \sqrt{8}A_7}$
Astigmatism	$A_a = 2\sqrt{6}[(A_5 - \sqrt{15}A_{12})^2 + (A_6 - \sqrt{15}A_{13})^2]^{1/2}$	$\theta_a = \dfrac{1}{2}\arctan\dfrac{A_6 - \sqrt{15}A_{13}}{A_5 - \sqrt{15}A_{12}}$
Defocus	$A_d = 2\sqrt{3}A_4 - 6\sqrt{5}A_9 - A_a/2$	
Coma	$A_c = 3\sqrt{8}\sqrt{A_7^2 + A_8^2}$	$\theta_c = \arctan\dfrac{A_7}{A_8}$
Spherical	$A_s = 6\sqrt{5}A_9$	

symmetry of the system, the Seidel terms of the wave aberration can be expressed as

$$W_{\text{Seidel}} = A_d r^2 + A_s r^4 + A_t r \cos(\theta - \theta_t) + A_a r^2 \cos(\theta - \theta_a) + A_c r^3 \cos(\theta - \theta_c). \quad (16)$$

By rearranging and grouping the Zernike polynomials, we obtain the magnitude and the angle of the Seidel terms.[26,27] Table 2 lists the Seidel coefficients as a function of the Zernike coefficients.

3. ACCURACY AND LIMITATIONS OF THE PROCEDURE

The precision of the wave aberration of the cornea obtained with the procedure described above is limited by different factors: accuracy of videokeratoscope devices to measure the surface elevation, numerical accuracy of the fitting method to Zernike polynomials, fourth-order approximations in the wave-aberration expansion, and experimental errors. In this section we study the impact of each of these factors, determining the accuracy and limitations of the complete procedure and establishing a range in which one may expect accurate results for the corneal aberrations.

To obtain the corneal shape, we used a MasterVue corneal topography system, manufactured by Humphrey Instruments. It is based on projection on the cornea of 20 Placido rings and posterior recording of the reflected light by a video camera. An algorithm reconstructs the corneal shape from the image of the rings by means of a double iterative method that forces the convergence of both the radial and the axial positions,[28] providing the values of corneal elevation (z_i) and curvature (R_i) in each of the points (r_i, θ_i) distributed in 20 rings and 180 meridians [see Fig. 2(b)].

A. Accuracy of the Videokeratoscope

To test the videokeratoscope, we measured conic surfaces with the following characteristics: four spheres with radius of 7.02, 7.94, 8.00, and 9.37 mm and three ellipsoids with radius and asphericities of $R = 7.03$ mm, $K = 0.6$; $R = 7.99, K = 0.8278$; and $R = 9.37, K = 0.6$. Test surfaces were calibrated by profilometry and interferometry with a root-mean-square error (RMSE) $< 0.09\ \mu$m (see Ref. 13 for details). Surfaces were positioned with a three-dimensional micrometric stage in front of the videokeratoscope. The reference elevation of each calibrated conic surface was first obtained from its radius and asphericity,

$$z(r_i) = \frac{R - (R^2 - K^2 r_i^2)^{1/2}}{K^2}, \quad (17)$$

at each point of the sample, where r_i is the radial position. With the N values of corneal elevations, z_i, obtained from the videokeratoscope and the values obtained with Eq. (17), the RMSE was calculated as

$$\text{RMSE} = \left\{ \frac{1}{N} \sum_{i=1}^{N} [z_i - z(r_i)]^2 \right\}^{1/2}. \quad (18)$$

Since the topographer used provides two independent sets of data, elevation, and curvature, we also evaluated the RMSE by using the new elevations obtained from the values of curvature.[13]

Figure 3 shows the calculated RMSE's, both from direct elevations and from curvatures, for six of the calibrated surfaces (three spheres and three ellipsoids) as a function of the distance to the axis. The two sets of values for the RMSE are similar, which is in agreement with the exigencies of convergence in the double iterative algorithm in the MasterVue system.[28] The error is highest for the surfaces with the largest radius, which indicates that probably the algorithm is optimized for the typical radius of the cornea (7–8 mm). As a general conclusion, the RMSE increases as the radial distance increases. However, the RMSE is never higher than 3 μm for an aperture of 8 mm in diameter; for a central area of 4 mm in diameter, the RMSE is lower than 1 μm. In a similar analysis for a TMS-1 corneal topographer, Applegate *et al.*[13] found RMSE's within 5–10 μm for a 6-mm-diameter aperture and RMSE's ~2 μm for 4 mm in diameter.

To test the topographer with nonrotationally symmetric surfaces, the calibrated surfaces were also measured placed at different angles with respect to the topographer.

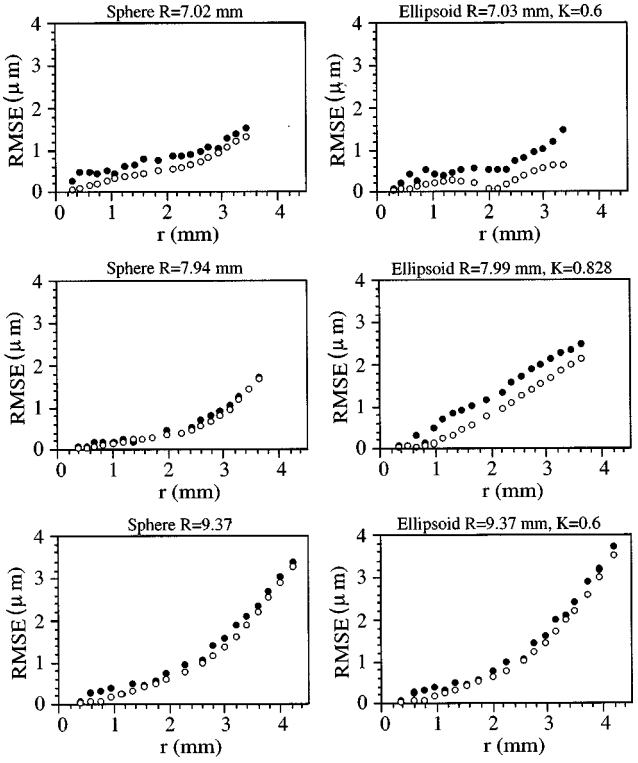

Fig. 3. RMSE between the actual values of surface elevation and the measured values for each ring of the MasterVue system, for six calibrated surfaces. The horizontal axis represents the radial average distance from each ring to the vertex of the surface. Solid circles, RMSE from the MasterVue elevation file; open circles, from elevations calculated from the MasterVue curvature file.

Table 3. Radius of Curvature and Asphericity of Six Calibrated Surfaces Estimated from Videokeratoscopic Data, in Comparison with the Actual Values, by Use of 15 and 20 Rings of the MasterVue System

Actual		Calculated			
		15 Rings		20 Rings	
R (mm)	K	R (mm)	K	R (mm)	K
7.02	1	7.011	1.007	7.013	1.009
7.94	1	7.941	1.015	7.939	1.020
9.37	1	9.372	1.031	9.376	1.092
7.03	0.6	7.031	0.593	7.031	0.584
7.99	0.828	7.977	0.814	7.956	0.808
9.37	0.6	9.366	0.602	9.365	0.602

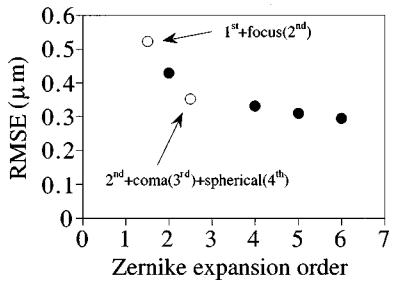

Fig. 4. RMSE between the measured corneal elevations and the elevations given by Eq. (9), for the fitting of the central area (5 mm in diameter) of a cornea as a function of the order of the Zernike expansion. Open circles represent an expansion with four terms (first-order plus second-order focus term) and an expansion with nine terms (second-order plus third-order cylindrical terms plus fourth-order spherical term).

Elevations obtained were in agreement with the expected results for each angle, with RMSE values similar to those shown in Figure 3.

B. Numerical Accuracy of the Fitting Method

We fitted the calibrated surfaces to Zernike polynomials and calculated the curvature radius and asphericity from the Zernike coefficients.[29] Table 3 presents these results in comparison with the actual data. Values were calculated within the area covered both by the 20 Placido rings and by only the first 15 rings. The largest discrepancies in the estimation of radius and asphericity appear when all the information is used. Taking the N values z_i provided by the videokeratoscope and the elevations calculated with Eq. (9), the RMSE of the fitting is

$$\mathrm{RMSE} = \left\{ \frac{1}{N} \sum_{i=1}^{N} \left[z_i - \sum_{j=1}^{L} a_j Z_j(\rho_i, \theta_i) \right]^2 \right\}^{1/2}. \quad (19)$$

Within an area of 5 mm in diameter, the RMSE's of the fitting with 15 terms (fourth order) were lower than 0.2 μm. That value is of the same order as the fabrication error of the surfaces.

We also calculated the RMSE's for the fitting of a cornea when a central area of 5 mm in diameter was modeled with different orders in the Zernike expansion (see Fig. 4). The values of the RMSE obtained (lower than 0.35 μm for third order and higher) indicate that the accuracy with which the corneal surface is estimated is limited by the videokeratoscope and not by the fitting routine, since the error of the measurement device is 1 μm for the same area. On the other hand, Fig. 4 shows that the value of the RMSE decreases slowly beyond the fourth order (15 terms), and the reduction is low from 9 terms (second order, plus the third-order cylindrical terms, plus the fourth-order spherical term) to 15 terms. These results indicate that, for normal corneas, the lower-order Zernike polynomials carry most of the information, in particular, the terms corresponding to the Seidel aberrations.

When the number of sampled points is large, polynomials V_j tend to the Zernike polynomials. Therefore the coefficients calculated for the Zernike expansion are practically independent of the number of terms employed. That occurs for the number of points we used. Table 4 shows the coefficients for the fitting of a cornea by use of the first 4, 6, 9, or 15 Zernike polynomials. When including new terms, the first coefficients (except piston, which is not relevant) remained practically constants.

C. Accuracy in the Estimation of the Wave Aberration

An error arises in the wave aberration owing to the RMSE associated with the corneal shape measurements. To evaluate the impact of this error on the estimation of the corneal aberrations, we now consider, for simplicity, the case of an object on axis at infinity. The surface base of the cornea is

$$z = \left[\frac{r^2}{2R} + \frac{{K_0}^2 r^4}{8R^3} \right] + \frac{(K^2 - {K_0}^2) r^4}{8R^3} = \left[\frac{r^2}{2R} + \frac{{K_0}^2 r^4}{8R^3} \right] + \frac{A_s}{(n - n')} \frac{r^4}{{r_0}^4}, \quad (20)$$

where K_0 is the ideal asphericity [Eq. (15)]. The term within brackets determines the position of the image plane, and the second term corresponds to the spherical

Table 4. Zernike Coefficient Values When a Corneal Surface Is Modeled with the 4, 6, 9, or 15 First Terms Listed in Table 1

Zernike Coefficient	Zernike Coefficient Values (mm)			
	First 4	First 6	First 9	First 15
a_1	0.010820	0.000532	0.000757	0.000821
a_2	0.000851	0.000817	0.000954	0.000954
a_3	0.000368	0.000352	0.000381	0.000381
a_4	0.157641	0.158260	0.158791	0.157987
a_5		−0.007624	−0.007841	−0.007772
a_6		0.003078	0.003146	0.003241
a_7			0.000471	0.000498
a_8			0.000166	0.000152
a_9			0.001218	0.001208
a_{10}				−0.000780
a_{11}				−0.000005
a_{12}				0.000057
a_{13}				−0.000025
a_{14}				0.000018
a_{15}				−0.000006

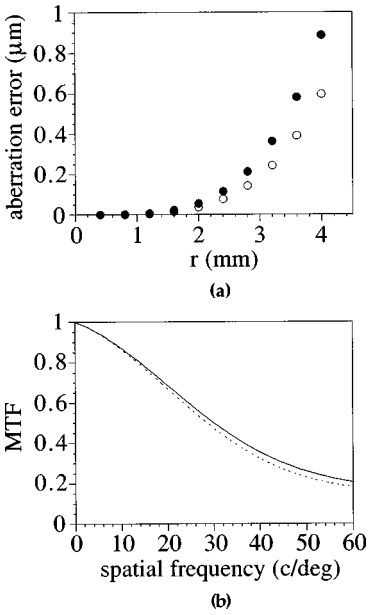

Fig. 5. (a) Error in the spherical aberration when calculated from the surface elevation measured with the MasterVue system, as a function of the distance to the axis, for two calibrated surfaces. Solid circles, sphere (R = 7.94 mm); open circles, ellipsoid (R = 7.99 mm and K = 0.828). The value n' = 1.3375 was used to calculate the aberration. (b) Modulation transfer function for the spherical surface mentioned in (a), calculated with the actual wave aberration (solid curve) and the estimated wave aberration (dotted curve). Pupil diameter, 4 mm.

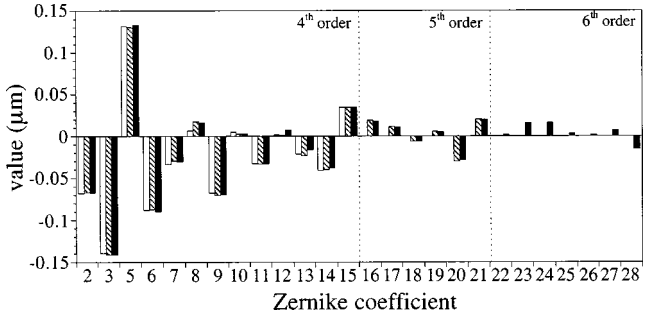

Fig. 6. Zernike coefficient values corresponding to the wave aberration of a cornea, calculated up to fourth-order (white bars), fifth-order (gray bars), and sixth-order (black bars).

aberration. Therefore, if the estimate of the elevation (z) is not correct, a fraction of the RMSE is transferred to the wave aberration as defocus. Figure 5(a) represents the error in the spherical aberration that is due to the RMSE in the elevation of two calibrated surfaces. Although the error in the elevation increases approximately linearly (see Fig. 3), the error in the spherical aberration is low for small apertures. For instance, the RMSE is 1.5 μm for the calibrated sphere (R = 7.94 mm) at r_0 = 3.5 mm, and the corresponding error in the spherical aberration result is 0.5 μm, approximately $(n - n') \times$ RMSE. But for r_0 = 2 mm the RMSE is 0.4 μm and the error in the aberration is only 0.05 μm, almost three times lower than $(n - n') \times$ RMSE. This indicates that the multiplication[13] of the RMSE by the factor $(n - n')$ overestimates the error in the aberration for small apertures, since part of the RMSE implies an image-plane displacement that is not relevant to the image quality. Figure 5(b) shows the modulation transfer function calculated[30] for the sphere for a 4-mm-diameter pupil, from the actual and measured values of spherical aberration. Differences between the two curves were small.

To determine the error that arose when the Taylor expansion of the square roots in Eqs. (2) and (3) was taken up to fourth order, we calculated the wave aberration in Zernike polynomials of a cornea by using both methods mentioned—elevation data fitting with posterior calculus of the aberration with Eq. (14) and fitting of the exact aberration values from Eq. (1). For a pupil of 4 mm in diameter, the resulting error was lower than 0.003 μm (differences between each pair of Zernike coefficients were lower than 0.001 μm), and for 8 mm in diameter, the error was ~0.2 μm. This indicates that both Eqs. (4) and (14) are accurate enough if the previous limitations are considered.

Figure 6 shows the Zernike coefficients of the wave aberration of a cornea when fourth-, fifth-, and sixth-order expansions are used. Higher-order coefficients are very small, and the first coefficients are similar if more terms are added.

D. Experimental Errors

We compared the results obtained from four sets of data measured in a calibrated sphere and in an astigmatic cornea. Figures 7(a) and 7(b) show the mean value and the standard deviation of the first 15 Zernike coefficients representing the surfaces, for a pupil of 4 mm in diameter. As one should expect, in the case of the calibrated sphere every coefficient is approximately zero except a_4 and a_9 (curvature and asphericity). From those coefficients we obtained $R = 7.9902 \pm 0.0358$ mm and $K = 1.0016 \pm 0.0182$, in good agreement with the reference data.

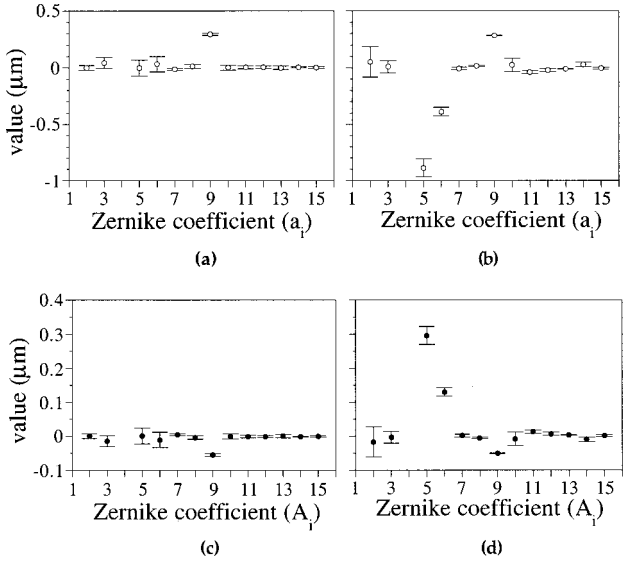

Fig. 7. (a) Mean value and error bars (two standard deviations), from four videokeratographs, of the first 15 Zernike coefficients representing a calibrated spherical surface (R = 8 mm), for a 4-mm-diameter pupil. (b) Same as (a), except for a cornea. (c) Mean value and error bars (two standard deviations) of the Zernike coefficients corresponding to the wave aberration calculated from the data of (a). (d) Same as (c), except for the wave aberration of the cornea of (b).

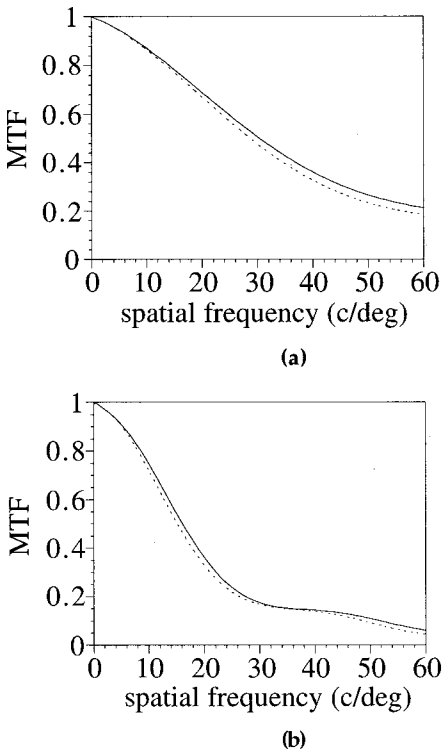

Fig. 8. (a) MTF from the wave aberration of the sphere of Fig. 7(c), calculated with the mean values of the Zernike coefficients (solid curve), and with the mean values plus two standard deviations (dotted curve). (b) Same as (a), except for the cornea of Fig. 7(d).

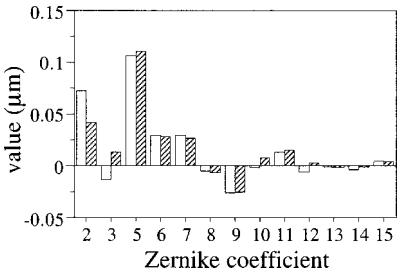

Fig. 9. First 15 Zernike coefficients for the corneal wave aberration calculated in a subject when the subject was instructed to blink before recording the videokeratography (white bars) and not to blink during the preceding 5 s (gray bars).

The error intervals were lower than 0.1 μm for the sphere. The interval of variability for the cornea was also small, with standard deviations lower than 0.1 μm, except for the tilt coefficient, a_2, with a standard deviation of 0.15 μm. This larger error is reasonable because of the right–left motion of the head, and it is not relevant for the wave-aberration estimation.

An error interval of $\sim$0.2 μm appears in the estimation of the surface elevation as a result of that variability. This value is five times lower than the RMSE that resulted from the videokeratoscope for the same aperture. That means that the limitation of the procedure is imposed by the instrument, as previously mentioned. Figures 7(c) and 7(d) show the mean values of the Zernike coefficients corresponding to the wave aberration (for 4-mm diameter) calculated from the previous elevations. Figures 8(a) and 8(b) represent modulation transfer functions calculated for the cornea and the calibrated surface, with the mean values of the aberration Zernike coefficients and with the mean values plus the experimental error. Differences between each pair of curves were nearly negligible.

E. Effect of the Posterior Surface of the Cornea

The posterior surface of the cornea has not been considered in this study. This surface separates two media with similar refractive indices and contributes to a small fraction of the eye power. We used the geometry of the anterior surface, using the separation of air ($n = 1$) and aqueous humor with an effective refractive index ($n' = 1.3375$) to calculate the aberrations of the complete cornea. To consider somehow the effect of both surfaces, a group of authors has proposed for the humor an effective refractive index that depends on the radial coordinate.[31] However, since we do not have access to accurate geometrical data from the second surface, we prefer to neglect it (assuming a certain interval of error) rather than assuming an incorrect posterior corneal shape. To estimate the error associated with this approximation, we considered a typical cornea with the following parameters:

- First surface[9]: $R = 7.8$ mm and $K = 0.9$, separating refractive indices 1 and 1.3771.
- Second surface: $R = 6.5$ mm and $K \in [0.632, 0.894]$, separating 1.3771 and 1.3374.

With this interval for the values of asphericity of the posterior corneal surface, the prediction of the schematic eye of Liou and Brennan[2] lies within the range of empirical results for the spherical aberration. Considering the two-surface model, the Zernike coefficient for the corneal spherical aberration is then within the interval $A_9 = [-0.037, -0.046]$ μm, whereas with the one-surface simple model the coefficient is -0.039 μm. This indicates that the error from the model that we assumed is similar to the indeterminacy that arises when both surfaces are considered, since the exact asphericity for each subject is unknown.

F. Influence of the Tear Film

The first interface that refracts the light coming into the eye is the tear film covering the cornea. Probably the surface measured by the videokeratoscope is the tear film instead of the anterior surface of the cornea. On the other hand, a problem could arise if tear instability changes the measurements, in particular, if the tears break up during the recording of the videokeratography. Figure 9 shows the values of the Zernike coefficients obtained in a subject from measurements under two different conditions: normal, when the subject just blinked before the recording (producing a normal tear film), and keeping the eye opened during several seconds without blinking (producing a more deteriorated tear film). Differences between the two sets of results are relatively small, which indicates that the method is robust against a possible break in the tear film. However, if the time for the nonblinking is sufficient to allow the tear film to break up, it is not possible to record the videokeratogra-

phy, owing to the low contrast in the images of the Placido rings. This ensures that all measurements were made with normal tear film.

4. SUMMARY AND CONCLUSIONS

We have described a complete procedure to calculate the wave aberration of a refracting surface from the elevation data. The wave aberration was calculated as the difference in optical path between the marginal rays and the chief ray refracted at the surface. We have obtained a general analytical expression truncating up to fourth order the square roots of the distances. The procedure is general and permits calculation of the aberrations of a given surface for objects both on axis and off axis. For aspheric surfaces we reobtained the known Seidel aberrations for objects off axis generalized for objects at any location on the plane (using a description with sine and cosine). For nonrotationally symmetric surfaces, we obtained the aberrations as the addition of radial symmetry terms and some asymmetric terms. In the wave-aberration expression, some nonlinear and crossed terms appear that could be important. The term $Mr^2\Delta z$ in expression (8) indicates that, for example, a tilt in the surface produces coma, or an astigmatic surface generates fourth-order aberrations with angular dependency. In practice, the calculation of the wave aberration by multiplying by $(n - n')$ the residual elevations after subtracting a reference conic from the measured elevations may be used as an approximation, which neglects some aberration terms. However, the complete expression [see Eqs. (6) and (8)] must be applied if a higher accuracy is required. The equations derived here are useful for different cases such as objects on axis, objects at infinity, spherical refracting surfaces, aspheric surfaces, and plane-parallel plate. etc.; the equations may be reiterated if more than one surface is present in the optical system.

The shape elevation map of the corneal surface was obtained from videokeratoscopy and fitted to a Zernike polynomial expansion. To calculate the expansion coefficients, a Gram–Schmidt orthogonalization, constructing intermediate orthogonal polynomials over a discrete and finite sample, was carried out. The wave aberration was obtained also as a Zernike polynomial representation. Several potential sources of inaccuracy are present in this methodology: experimental errors due to defocus error, misalignments, or movements; inaccuracy of the Zernike fitting method; approximations in the square roots to calculate the wave aberration; and assumptions intrinsic to the videokeratoscopic devices. The last one is the greatest limitation of the procedure. We tested the accuracy of the videokeratoscope by measuring calibrated surfaces with a MasterVue system, and we found an RMSE of 1–2 μm for an aperture of 4–6 mm in diameter, whereas the RMSE associated with the experimental errors and with the fitting method was 0.2 μm. Experimental variability was small, indicating that this device is not very sensitive to alignment or defocus errors, although other devices could present larger errors.[14]

A fourth-order Zernike expansion (15 terms) is a good approximation to the normal human cornea for pupils of 4–6 mm in diameter. For abnormal corneas (after radial keratotomy, for instance[32]), higher-order terms should be included. If an exact method to determine the corneal elevations is available, the inclusion of additional terms is suggested to improve the accuracy (for instance, with 45 terms, up to eighth order, the RMSE of the fitting decreased to 0.02 μm[22]). Approximations up to fourth order in the Taylor expansion of the square roots in the wave aberration are accurate for typical corneal dimensions.

Several researchers have studied the accuracy of different systems to measure the corneal shape. In general, they found that the error in the estimation of the corneal elevation increased with increased radial position and when the surface differed from a sphere. Greivenkamp *et al.*[14] compared the capabilities of three videokeratoscopes (EyeSys, TMS-1, EH-270) to measure toric surfaces with curvature radius of 7.8 mm, finding that the three instruments present a systematic error in detecting the amount of astigmatism. For instance, for a five-dimensional astigmatic surface the RMSE is 1.5–1.7 μm with the TMS-1 and EH-270 and 7.5 μm with the EyeSys, for apertures of 8 mm in diameter. For nonastigmatic surfaces (sphere) they found a RMSE ~0.6–0.8 μm (lower than the 2 μm we found in the sphere of 7.94-mm radius for a similar area). Applegate *et al.*[13] discussed whether the surface elevation measured with videokeratoscopes may be used to estimate the corneal wave aberration accurately. For a TMS-1 system they found a RMSE elevation measurement of ~5 μm for a pupil of 8 mm in diameter and fixated an error for the aberration of 0.3375 times this RMSE, i.e., approximately 2 μm, which is a high value when compared with the typical aberration of the normal eye. With the MasterVue system the RMSE is 3 μm or smaller for the 8-mm-diameter pupil, and therefore the error in the aberration is ~1 μm. On the other hand, we have demonstrated that a fraction of the RMSE in determining the surface shape affects defocus, especially for small pupils. For a 4-mm-diameter pupil, the error in the spherical aberration is 0.05 μm, whereas the spherical aberration is ~0.5 μm for the eye[33] or 0.4 μm for the cornea[9] for the same pupil.

In conclusion, the complete method presented here is applicable with sufficient precision to calculate the wave aberration of the cornea from videokeratoscopic data over an area of 4–6 mm in diameter. The accuracy of the procedure is limited by the error of the videokeratoscopes to obtain the corneal elevation. This error depends on the corneal topography system used and should be tested in each case to determine the range of precision. Since the error is a systematic one, increasing from center to periphery, comparative studies of the corneal aberrations may be extended to larger pupils. In the future the accuracy of determining with this procedure the actual wave aberration of an individual cornea will be better if videokeratoscopes with improved capabilities or new corneal topography devices providing more accurate measurements are available.

ACKNOWLEDGMENTS

This research was partially supported by grants to P. Artal from Pharmacia and Upjohn Groningen (The Nether-

lands) and Dirección General de Enseñanza Superior (Spain) (grant PB97-1056). The authors thank Raymond Applegate (University of Texas, San Antonio) for lending us reference-calibrated surfaces and Charlie Campbell (Humphrey Instruments) for providing us with the software for access to the corneal elevation data.

REFERENCES AND NOTES

1. P. Artal and A. Guirao, "Contributions of the cornea and the lens to the aberrations of the human eye," Opt. Lett. **23**, 1713–1715 (1998).
2. H. L. Liou and N. Brennan, "Anatomically accurate, finite model eye for optical modeling," J. Opt. Soc. Am. A **14**, 1684–1695 (1997).
3. J. Schwiegerling and J. E. Greivenkamp, "Keratoconus detection based on videokeratoscopic height data," Optom. Vision Sci. **73**, 721–728 (1996).
4. J. Schwiegerling, "Cone dimensions in keratoconus using Zernike polynomials," Optom. Vision Sci. **74**, 963–969 (1997).
5. R. D. Applegate, G. Hilmantel, and H. C. Howland, "Corneal aberrations increase with the magnitude of radial keratotomy refractive correction," Optom. Vision Sci. **73**, 585–589 (1996).
6. K. M. Oliver, G. P. Hemenger, M. C. Corbett, D. P. S. Obrant, S. Verna, J. Marshall, and A. Tomlinson, "Corneal optical aberrations induced by photorefractive keratoctomy," J. Refrac. Surg. **13**, 246–254 (1997).
7. S. G. El Hage and F. Berny, "Contribution of the crystalline lens to the spherical aberration of the eye," J. Opt. Soc. Am. **63**, 205–211 (1973).
8. A. Tomlinson, R. P. Hemenger, and R. Garriott, "Method for estimating the spherical aberration of the human crystalline lens in vivo," Invest. Ophthalmol. Visual Sci. **34**, 621–629 (1993).
9. P. M. Kiely, G. Smith, and L. G. Carney, "The mean shape of the human cornea," Opt. Acta **29**, 1027–1040 (1982).
10. T. C. A. Jenkins, "Aberrations of the eye and their effects on vision: part 1," Br. J. Physiol. Opt. **20**, 59–91 (1963).
11. R. P. Hemenger, A. Tomlinson, and K. Oliver, "Optical consequences of asymmetries in normal corneas," Ophthalmic Physiol. Opt. **16**, 124–129 (1996).
12. T. W. Raasch, "Corneal topography and irregular astigmatism," Optom. Vision Sci. **72**, 809–815 (1995).
13. R. A. Applegate, R. Nuñez, J. Buettner, and H. C. Howland, "How accurately can videokeratographic systems measure surface elevation?" Optom. Vision Sci. **72**, 785–792 (1995).
14. J. E. Greivenkamp, M. D. Mellinger, R. W. Snyder, J. T. Schwiegerling, A. E. Lowman, and J. M. Miller, "Comparison of three videokeratoscopes in measurements of toric tests surfaces," J. Refract. Surg. **12**, 229–239 (1996).
15. R. L. Schultze, "Accuracy of corneal elevation with four corneal topography systems," J. Refract. Surg. **14**, 100–104 (1998).
16. J. Schwiegerling and J. E. Greivenkamp, "Using corneal height maps and polynomial decomposition to determine corneal aberrations," Optom. Vision Sci. **74**, 906–916 (1997).
17. V. N. Mahajan, *Aberration Theory Made Simple* (SPIE Optical Engineering Press, Bellingham, Wash., 1991).
18. The Taylor expansion of a function with three variables is given by $f(\mathbf{x}) = \Sigma_{k=0}^{\infty}(1/k!)f^{(k)}(\mathbf{x}_0)$, with $\mathbf{x} = (X, Y, Z)$, $\mathbf{x}_0 = (0, 0, 0)$, and $f^{(k)}(\mathbf{x}) = (\mathbf{x}\nabla)^k f(\mathbf{x})$.
19. T. O. Salmon and D. G. Horner, "Comparison of elevation, curvature, and power descriptors for corneal topographic mapping," Optom. Vision Sci. **72**, 800–808 (1995).
20. J. Y. Wang and D. E. Silva, "Wave-front interpretation with Zernike polynomials," Appl. Opt. **19**, 1510–1518 (1980).
21. M. Born and E. Wolf, *Principles of Optics* (Pergamon, New York, 1985).
22. J. Schwiegerling, J. E. Greivenkamp, and J. M. Miller, "Representation of videokeratoscopic height data with Zernike polynomials," J. Opt. Soc. Am. A **12**, 2105–2113 (1995).
23. C-J. Kim and R. R. Shannon, "Catalog of Zernike polynomials," in *Applied Optics and Optical Engineering*, R. R. Shannon and J. C. Wyant, eds. (Academic, San Diego, Calif., 1987), Vol. X, Chap. 4. (Note that the ordering of the polynomials in the list is not universally accepted; here we used a different ordering.)
24. D. Malacara, J. M. Carpio-Valadéz, and J. J. Sánchez-Mondragón, "Wavefront fitting with discrete orthogonal polynomials in a unit radius circle," Opt. Eng. **29**, 672–675 (1990).
25. S. N. Bezdid'ko, "Calculation of the Strehl coefficient and determination of the best-focus plane in the case of polychromatic light," Sov. J. Opt. Technol. **42**, 514–516 (1975).
26. G. Conforti, "Zernike aberration coefficients from Seidel and higher-order power-series coefficients," Opt. Lett. **8**, 407–408 (1983).
27. R. K. Tyson, "Conversion of Zernike aberration coefficients to Seidel and higher-order power-series aberration coefficients," Opt. Lett. **7**, 262–264 (1982).
28. C. Campbell, "Reconstruction of the corneal shape with the MasterVue corneal topography system," Optom. Vision Sci. **74**, 899–905 (1997).
29. By comparing Eqs. (9) and (5), we can calculate the curvature and asphericity from the Zernike coefficients as

$$R = \frac{{r_0}^2}{2(2\sqrt{3}a_4 - 6\sqrt{5}a_9 - 30\sqrt{7}a_{22} + \cdots)},$$

$$K^2 = \frac{8R^3}{{r_0}^4}(6\sqrt{5}a_9 - 30\sqrt{7}a_{22} + \cdots),$$

where r_0 is the maximum radial extent of the surface.
30. J. W. Goodman, *Introduction to Fourier Optics*, 2nd ed. (McGraw-Hill, New York, 1996).
31. R. P. Hemenger, A. Tomlinson, and K. Oliver, "Corneal optics from videokeratographs," Ophthalmic Physiol. Opt. **15**, 63–68 (1995).
32. R. A. Applegate, H. C. Howland, J. Buettner, A. J. Cottingham, Jr., R. P. Sharp, and R. W. Yee, "Radial keratotomy (RK), corneal aberrations and visual performance," Invest. Ophthalmol. Visual Sci. **36**, S309 (1995).
33. I. Iglesias, E. Berrio, and P. Artal, "Estimates of the ocular wave aberration from pairs of double-pass retinal images," J. Opt. Soc. Am. A **15**, 2466–2476 (1998).